# Accepted Manuscript

Effects of cooling temperature profiles on the monoglycerides oleogel properties: A rheo-microscopy study

Camila Palla, Juan de Vicente, María Elena Carrín, María José Gálvez Ruiz

Please cite this article as: C. Palla, J. de Vicente, M.E. Carrín, et al., Effects of cooling temperature profiles on the monoglycerides oleogel properties: A rheo-microscopy study, Food Research International, https://doi.org/10.1016/j.foodres.2019.108613

**Effects of cooling temperature profiles on the monoglycerides oleogel properties: a rheo-microscopy study**

Camila Palla[a,b,*] cpalla@plapiqui.edu.ar, Juan de Vicente[c], María Elena Carrín[a,b], María José Gálvez Ruiz[c]

[a]Departamento de Ingeniería Química, Universidad Nacional del Sur (UNS)

[b]Planta Piloto de Ingeniería Química - PLAPIQUI (UNS-CONICET), 8000, Bahía Blanca, Argentina

[c]Departamento de Física Aplicada and Excellence Research Unit "Modeling Nature" (MNat), Universidad de Granada, 18071, Granada, Spain

[*]Corresponding author.

**Abstract**

The oleogelation process has become in a great interest area for the food sector. The aim of this study was to understand the effect of cooling temperature profiles (CTP) applied during oleogelation on microstructure and some macroscopic properties of monoglycerides (MG) oleogels. To this purpose, oleogels from MG and high oleic sunflower oil were produced using programed CTP corresponding to the actual temperature evolution of the samples when they are left at rest to progress in a specific ambient temperature (AT). In order to evaluate the crystal formation during the gelation process, a torsional rheometer equipped with a rheo-microscope (RM) module was used. This allowed us to carry out simultaneously rheological measurements and record images of the gels during their formation process. Overall, microstructural characteristics were determined: fractions of crystalline material and oil, crystal length and shape, the Avrami index, and the fractal dimension. Although crystal formation took place during a similar range of temperatures (~55 - 46 $^{o}$C), significant morphological differences in the distribution and size of crystal and aggregates were observed depending on the applied CTP, and the area occupied by the crystals and oil phase did not depend on CTP used. RM images were useful to follow the kinetics of crystallization as well as to identify a more restricted time domain in the rheological behavior allowing to find more accurate Avrami index values. Furthermore, the analysis of RM images turned out to be an efficient approach to obtain accurate measurements of the fractal dimension. High fractal dimension values were associated with gels exhibiting high number of homogeneous small crystals. Oleogels composed by this network generated a material with high capacity to retain oil. A weak-link regime approach applied to the dynamic systems was appropriate to describe the relationship between the elastic modulus and the crystal formation during the oleogels structuration. In conclusion, these findings may serve to the food industry to achieve a better understanding of the oleogelation process that allows it to control the quality of obtained oleogels, which could be utilized to replace and/or reduce the *trans* and saturated fats in food formulations.

Keywords: Oil structuration; Rheology; Images analysis; Microstructure; Modified Avrami model; Fractal dimension; Weak-link regime model

**Abbreviations**

AT      ambient temperature

CLSM  confocal laser scanning microscopy

CTP     cooling temperature profile

D       mass fractal dimension

$D_{bc}$     box counting fractal

D50     median particle size

F       reduced crystallinity

G'      elastic modulus

G"      viscous modulus

GLC     gas-liquid chromatography

Ha      hardness

HOSO refined high oleic sunflower oil

MG      monoglycerides

OBC     oil binding capacity

PAF     pore area fraction

PLM     Polarized light microscopy

RM      rheo-microscope

$Y_s$      crystalline solid volume formed until a given time

$Y_{max}$    maximal crystal phase volume

η*      complex viscosity

$k_{app,}$ $t_0$, and $n$ apparent rate constant, induction time, and Avrami exponent of the modified Avrami model      respectively

Φ       volume fraction of solid fat

$m$ and $γ$      constants of the weak-link regime model

# 1. Introduction

Today, the food industry rise to new challenges bringing to a great attention on novel healthy products. This increasing interest is a consequence of the novel exigencies of the consumers and the requirements of the international institutions as Food and Drug Administration (FDA). In particular, new ingredients and processes need to be investigated to achieve the reduction of the level of saturated and *trans* fatty acids in food products, since the high intake of these fats is considered unhealthy due to their links to increased risk of cardiovascular diseases, obesity, and diabetes (Dhaka & Gulia, 2011; Souza et al., 2015). In relation to this, on 17 June 2015, the FDA determined that partially hydrogenated oils were no longer GRAS (generally recognized as safe) and need to be removed from food products by June 2018 (Doan, Tavernier, Okuro, & Dewettinck, 2018; Gaudino, Ghazani, Clark, Marangoni, & Acevedo, 2019). The main complication related to the removal of solid fats from food formulations derives from their melting and crystallization behavior, which are responsible for functional attributes such as texture, plasticity, and shelf life (Dassanayake, Kodali, & Ueno, 2011). If the solid fat fraction is simply replaced with an unsaturated fat, the final structure of the products cannot match the quality characteristics of the original products, such as textural characteristics, affecting sensory perception and consumer satisfaction (Doan et al., 2018; Gavahian, Tiwari, Chu, Ting, & Farahnaky, 2019). In this context, the oleogelation appears as a new and effective strategy to structure liquid oil into soft, solid-like systems (Doan et al., 2018; Ferro, Okuro, Badan, & Cunha, 2019). The potential use of these soft materials as fat replacers and product quality enhancers has been recently studied in the elaboration of ice creams, chocolate spread, sweet bread, cakes, cookies, muffins, frankfurts, pork patties, and sausages (Agregán et al., 2019; Fayaz et al., 2017; Giacomozzi, Carrín, & Palla, 2018; Singh, Auzanneau, & Rogers, 2017).

Oleogels are systems containing self-assembled structures entrapping liquid oil in a three-dimensional network (Hughes, Marangoni, Wright, Rogers, & Rush, 2009). These structures can be formed by low molecular components, polymeric substances or crystalline materials such as saturated MG, waxes, fatty acids, fatty alcohol, etc. In order to prepare an oleogel, a relative low amount of lipid structurant (gelator) is added to oil. With the appropriate processing, that includes heating, stirring, and cooling, the structurant molecules are dispersed in the oil phase to later form an intricate solid network that entraps the oil (O'Sullivan, Barbut, & Marangoni, 2016). It is interesting to note that oleogel physical properties are not only determined by the chemical composition of gel components and their relative amounts but also by the selected preparation conditions used for its formation. Therefore, these properties represent a

relevant aspect for the food industry because not only they define oleogel potential applications but also they can determine functional and organoleptic properties of oleogel-containing food products (Fayaz et al., 2017).

Physicochemical properties of oleogels composed by MG and different vegetable oils have been investigated by numerous techniques because they are especially suitable to obtain gels with plastic structures characteristics of hardstock fats widely used in food products (da Pieve, Calligaris, Co, Nicoli, & Marangoni, 2010; Ferro et al., 2019; Ho Lam & Rogers, 2011; Palla, Giacomozzi, Genovese, & Carrín, 2017). In particular, rheometry is a well-established technique to quantify the viscoelastic characteristics of complex soft materials such as the oleogels of interest in this manuscript (Chen & Terentjev, 2009; da Pieve et al., 2010; López-Martínez et al., 2014; Lupi et al., 2016; Ojijo, Kesselman, et al., 2004). The results of these investigations indicated that MG concentration and processing conditions (cooling and shear rates) affected significantly both the crystallization and mesoscopic organization of MG, and therefore the macroscopic physical characteristics of obtained oleogels. Image analysis is other useful tool to elucidate the structural features of crystalline networks. For example, Blake and Marangoni (2015) found that rapid cooling decreased both crystal length and network pore area fraction, and increased the fractal dimension of wax oleogels. The latter resulted in a rise of the ability of the oleogels to retain oil. Moreover, polarized light microscopy have been employed to follow the crystallization process and to determine both the nucleation type and the dimensionality of crystal growth in systems formed by 12-hydroxy stearic acid/stearic acid/trihydroxystearin and mineral oil (Rogers & Marangoni, 2008).

In this manuscript, we are especially interested in elucidating the importance of CTP on the MG oleogel formation. The cooling rate plays a critical role in its physical properties since it directly influences the nucleation and crystallization kinetics for the formation of the crystalline network (Rogers, Tang, Company, & Marangoni, 2008). In this context, it is important to note that the influence of a constant rate CTP has been extensively documented (López-Martínez et al., 2014; Lupi et al., 2016; Ojijo, Kesselman, et al., 2004; Ojijo, Neeman, Eger, & Shimoni, 2004). However, in practice, the molten samples are put into containers at AT and as a result, the samples exhibit a different (non-constant rate) CTP depending on the AT. A particularly relevant example is the work by Palla et al. (2017), who obtained oleogels from high oleic sunflower oil (HOSO) and a commercial mixture of MG (Myverol 18-50 XL PL) at different AT. The authors found that textural characteristics, rheological properties, and the capacity to retain oil were greatly affected by the particular AT used during processing. It is expected that next efforts in the oleogels field will be directed to translate the laboratory experiments

to industrial scale, and therefore the understanding of the relationship between the cooling process in oleogels production and obtained functionality will be essential.

Keeping the aforementioned perspective in mind, in the present research we study the effect of the CTP employed in the production of oleogels from MG and HOSO on the obtained microstructures and their relationship with macroscopic properties. In order to evaluate the crystal formation during the gelation process, a torsional rheometer equipped with a rheo-microscope (RM) module was used. With this, it becomes also possible to obtain microstructural parameters such as the Avrami index that allows us to determine the type of nucleation and dimensionality of the crystal growth process. Furthermore, a variety of complementary techniques such as confocal and conventional polarized optical microscopy, conventional rheology, and differential scanning calorimetry were used to determine the microstructural characteristics: fractions of crystalline material and oil in the oleogels, crystal length and shape, and the fractal dimension. Thus, the novelty of this work is the evaluation of the CTP effect on oleogel final properties, as a more realistic way to consider the formation process, and the use of rheo-microscopy as a new analysis tool to its study. Other innovative aspects of this contribution involve the use of the weak-link regime approach to obtain the fractal dimension during gelation process, as well as the use of Avrami model applied to RM images analysis and rheology to evaluate kinetics of crystallizations of MG oleogels produced under different CTP.

## 2. Materials and methods

### 2.1. Materials

Refined HOSO was bought at a local supermarket, being the weight composition of fatty acids determined as fatty acid methyl esters (FAME) by GLC analysis according to AOCS Official Methods Ce2-66 and Ce1-62 (AOCS, 2009): saturated fatty acids 6.58%, monounsaturated fatty acids 85.25%, and polyunsaturated fatty acids 7.71%. A commercial food grade mixture of monoglycerides with high content of monostearin, Myverol 18-08 NP, was generously donated by Kerry (Ireland), being its product specification: monoglycerides >90% purity grade - fatty acid composition obtained by GLC analysis as FAME: stearic acid 90.65%, palmitic acid 6.43%, and arachidic acid 1.53% - and melting point: 72.0 °C.

### 2.2. Samples preparation

Oleogel mixtures were prepared in a glass container system with a temperature-controlled water bath and controlled magnetic agitation. Oleogels were obtained solubilizing 10 wt% of MG in HOSO by heating at 75 °C, and constant stirring at 400

rpm during 30 min. The molten samples were then placed in the rheometer and subjected to the temperature treatments described in section 2.4.1 or put into cylindrical containers (30 ml) allowing to form the gels at a specified AT (5, 17.5, or 30 °C) under static conditions. In this last case, gelled samples were stored in darkness at 5 °C for 24 h until analysis.

## 2.3. Determination of cooling temperature profile (CTP)

In order to measure the change of temperature experienced by samples during the cooling process at AT, a k-type temperature probe was introduced into samples contained in the cylindrical containers to record their evolution over time from the preparation temperature (75 °C) to the specified AT. Later, each experimentally determined CTP was mathematically described by representing the observed exponential decay type behavior as the sum of consecutive piecewise linear line segments. As result, it was possible to obtain for each AT a series of time interval-temperature ramp that was used to develop the temperature programing later introduced in the rheometer and DSC software.

## 2.4. Analytical methods

### 2.4.1. Rheological and image monitoring of gelation process

A Paar Physica rheometer (model MCR502, Anton Paar, Austria) equipped with a RM module was used to simultaneously carry out rheological measurements and record images of the internal structures of materials during the gelation process. The RM module consisted of a CCD (charge-coupled device) camera, a long working distance objective (magnification 20x) and a microscope tube with a polarized filter. A parallel-plate geometry (40 mm diameter) with a bottom glass plate was used in the assays. The microscopic observation was carried out in the velocity gradient direction. A gap of 0.3 mm was set to allow visualization of structures. In order to replicate the samples real cooling process (determined in Section 2.3) in the rheometer, small-amplitude oscillatory shear (SAOS; strain 0.05% and frequency 10 rad/s) temperature sweep tests were carried out by programing each CTP in the rheometer software.

Additional rheological measurements were performed in a conventional Paar Physica rheometer (model MCR 301, Anton Paar GmbH, Austria) using a parallel-plate geometry (50 mm diameter) with a gap of 0.5 mm in order to obtain more precise measurements. Oscillatory temperature sweep tests (strain 0.05%, frequency 10 rad/s, within the linear viscoelastic region) were carried out by introducing each CTP in the rheometer programming.

Multiwave rheological assays were also carried out to precisely determine the gel point. It was performed according to the procedure described in detail by Shahrivar et al. (Shahrivar & de Vicente, 2014), but setting each CTP in the rheometer programming. All measurements were performed at least twice, using fresh molten samples from batches of oleogel prepared individually.

### 2.4.2. Microscopy additional techniques: Confocal laser scanning microscopy (CLSM) and Polarized light microscopy (PLM)

Once the rheological tests were completed, the samples were carefully removed from the rheometer bottom plate, placed on a microscope slide and stored at 5 °C for 24 h for further analysis. For CLSM, high-resolution optical images of samples were obtained using a Leica inverted confocal microscope (Leica Microsystems Heidelberg GmbH, Germany). Optical sections about 1µm deep were collected using a HCX PL APO CS 20.0x0.70 DRY UV objective upon illumination of the sample with a 488 nm argon laser bean. Images were processed with Leica confocal software. Furthermore, digital optical micrographs were taken with an OLYMPUS BX51 optical microscope with polarized light (Olympus, Japan) using a 20x objective lens and digital DP50 camera.

### 2.4.3. Microstructural analysis from images

All the obtained images were processed and analyzed using ImageJ software (National Institute of Mental health, ML, USA).

*2.4.3.1. Crystal size distribution*

Among 3 or 4 images of oleogels final state obtained from the RM, CLSM, and PLM were used to obtain the crystal length distribution in oleogels samples (Allen, 1997). The measuring tool of the software was calibrated using the corresponding scale for each kind of image. In every image, twenty measurements were taken and the total measurements were used to obtain a frequency histogram by Histogram tool of the Analysis ToolPak from Excel (Microsoft Office 2013). Results are reported in terms of the D50, the median, which is defined as the particle size where half of the population lies below this value, and the Span = (D90 – D10)/D50, which gives an indication of how far apart the 10 percent and 90 percent points are, normalized with the midpoint (HORIBA Scientific, 2010).

*2.4.3.2. Pore area fraction (PAF)*

A simple and effective method to characterize the crystalline structure of this type of oleogels is determining the area unoccupied by crystals, which is called pore area fraction (PAF). It was determined in a similar way as described by Blake and

Marangoni (Blake & Marangoni, 2015). In brief, the obtained images were converted to 8-bit type and transformed into the form of white objects on a black background. The area of white pixels in each image is indicative of the solid crystalline material and can be quantified by the former software. This way, the percentage of PAF was calculated as the remaining area.

### 2.4.3.3. The box counting fractal dimension

Fractal geometry is widely used in image analysis to describe complex forms found in nature. In particular, the fractal dimension parameter (D) is an index of the space-filling properties of an object and it can serve as an indicator of the crystal mass distribution in the oleogel network (Blake & Marangoni, 2015). This can be obtained by different computing methods such as the box counting method. We carried out this analysis through FracLac plugin from ImageJ on images converted into 8-bit binary images (Karperien, 2004). The box counting fractal dimension ($D_{bc}$) value was obtained as the average value from at least four processed images. Since the determination performed by image analysis is based on two-dimensional space, an extra dimension was added to the calculated $D_{bc}$ value (D= $D_{bc}$ +1) to actually represent the three-dimensional features of the gel (Dàvila & Parés, 2007).

### 2.4.3.4. Parameters of the modified Avrami model

Nucleation and dimensionality of crystal growth are essential factors in determining the physical properties of oleogel crystalline networks. For isothermal conditions, the crystallization kinetics is frequently modelled using the Avrami equation. However, some authors have found that it allows to appropriately describe experimental data obtained under non-isothermal conditions as well (Ho Lam & Rogers, 2011; Rogers & Marangoni, 2008). As consequence, a modified Avrami model has been proposed to be used (Ho Lam & Rogers, 2011):

$$\frac{Y_s}{Y_{max}} = 1 - e^{-k_{app}(t-t_0)^n} \qquad (1)$$

where $k_{app}$ is the apparent crystallization rate constant, t is the time, $t_0$ is the induction time, and $n$ is the Avrami index representing both the dimensionality of growth (1D, 2D, 3D) and the nucleation mode (sporadic or instantaneous) (Ho Lam & Rogers, 2011). $Y_s$ is the crystalline solid volume formed until a given time and $Y_{max}$ is the maximal crystal phase volume.

In order to quantify the amount of crystalline solid material during oleogel formation, the percentage of crystal area was determined in each RM image. It was performed using the Color Inspector 3D plugin which allows the generation of color histograms by segmentation of the color space presented in the images (Barthel, 2004). As a result, colors are identified - e.g. using RGB code - and their absolute and relative frequencies

are listed. In brief, the RM images were converted into 32-bit grey scale images and partitioned into 32 colors. From the histogram, the percentage of area corresponding to each segment was obtained. Based on visual inspection, segments were classified as crystalline structure or oil and their percentage of area were quantified adding each corresponding contribution. The variable used to follow the crystallization process was defined as:

$$\frac{Y_s}{Y_{max}} = \frac{\% \ crystal \ area \ (t)}{\% \ crystal \ area \ max.} \qquad (2)$$

The $k_{app}$, $t_0$, and $n$ parameters were obtained by nonlinear curve fit using OriginPro 9.1 software (OriginLab, USA).

### 2.4.4. Microstructural analysis from rheology

*2.4.4.1. Parameters of the modified Avrami model*

The crystalline network formation in similar systems has been monitored following the evolution of rheological parameters (Ho Lam & Rogers, 2011; Liu & Sawant, 2001; Rocha-Amador et al., 2014). In this work, the temperature sweep test was used to obtain the complex viscosity on time and thus the Avrami model parameters (from Equation 1) through the $Y_s/Y_{max}$ ratio defined as (Liu & Sawant, 2001):

$$\frac{Y_s}{Y_{max}} = \frac{\eta^*(t) - \eta_{solv}}{\eta^*_{max} - \eta_{solv}} \qquad (3)$$

where $\eta^*(t)$, $\eta^*_{max}$, and $\eta_{solv}$ denote the sample complex viscosity at time t, the maximum sample complex viscosity, and the complex viscosity of the solvent, HOSO, respectively.

*2.4.4.2. Fractal dimension based on the weak-link regime for colloidal dispersion*

The crystallization behavior of different fat systems was studied using the relationship of the elastic modulus (G') with the solid volume fraction (Φ) via the mass fractal dimension (D) of the network by applying a weak-link regime theory developed for colloidal gels having a high volume fraction of solids (Narine & Marangoni, 1999a; Toro-Vazquez, Dibildox-Alvarado, Charó-Alonso, Herrera-Coronado, & Gómez-Aldapa, 2002). In these systems, the G' increases as a function of Φ following a power-law behavior in the form:

$$G' = \gamma \ \Phi^m \qquad (4)$$

$$m = 1/(3 - D) \qquad (5)$$

where $m$ and $\gamma$ are constants to be determined experimentally and Φ can be assumed equal to the reduced crystallinity (F) (i.e. calculated by Equation 6 (Toro-Vazquez et al., 2002)). From the linearization of equation (4), the obtained slope $m$ can be used to find D. It is important to mention that, until now, this approach has been applied to isothermal systems of a given fat material by determining the G' value at a fixed

temperature for samples with different volume fractions of solid fat - e.g. different blends of the fat material and oil as diluent- (Narine & Marangoni, 1999b). Here, we used this approach to determine D in dynamic systems (non-isothermal process). In order to compute the evolution of fractal organization when monoglycerides crystallization took place during oleogel's cooling process, we correlated the F and G' values for the same time-temperature point, which was possible thanks to having applied an identical cooling process in the corresponding assays.

*2.4.4.2.1. Determination of the reduced crystallinity (F) by DSC*

Oleogels thermal behavior was analyzed using a Discovery DSC (TA Instruments, USA). An amount between 18-20 mg of previously prepared oleogel sample was sealed in aluminum hermetic pans and heated at 80 °C for 30 min to eliminate their thermal history. After that, the sample was cooled until the preparation temperature (75 °C at 5 °C/min) and then cooled following one of the previously determined CTP. This allows to obtain, in each case, the exothermic phase transition corresponding to the monoglycerides crystallization event. The reduced crystallinity associates the crystallinity of the system at a given time with the total crystallinity achieved under the experimental conditions (Toro-Vazquez et al., 2002). F values from the crystallization exothermic peak were calculated as:

$$F = \frac{\Delta H_t}{\Delta H_{tot}} \qquad (6)$$

where $\Delta H_t$, the cumulated enthalpy, is the area under the crystallization curve from the time where the process begins (time where the heat capacity of the sample has a significant departure from the baseline) up to time t and $\Delta H_{tot}$ is the total area under the crystallization curve. The TRIOS 4.1.1 (TA Instruments) software in combination with Excel was used to carry out the numerical integration of the obtained curves.

## 2.4.5. Oil binding capacity (OBC)

The oil binding capacity (OBC) was determined by quantifying the amount of oil retained by the sample after centrifugation (Giacomozzi et al., 2018). For that, a portion (about 1 g) of oleogel formed in the cylindrical container was carefully removed from there and placed in an eppendorf tube. Later, this was centrifuged at 9000 rpm for 15 min at 17 °C using a microcentrifuge (Giumelli z-127-D, Argentina) and the released oil was discarded. Five replicates of each sample were performed. The percentage of OBC was expressed as: (mass of retained oil/ mass of initial oleogel)*100.

## 2.4.6. Hardness

A Texture Analyzer TA Plus (Lloyd instruments, England) equipped with a 50 N load cell was used for textural evaluation. The texture profile analysis (TPA) test consisted of a two cycle penetration of the sample using a cylindrical probe with rounded head (12.5 mm in diameter) as it was described in a previous work (Palla et al., 2017). The test was carried out using the following parameters: 1 mm/s of crosshead speed, 10 mm of penetration distance, and 10 s of waiting time between the cycles. From the resulting force-time curve, the hardness was determined as the maximum force measured during the first penetration cycle. The data were analyzed by NEXYGEN Plus (Lloyd instruments, England) and OriginPro 9.1 (OriginLab, USA) software. Measurements were performed in the oleogels formed in the cylindrical containers after holding the samples at 24 °C for 15 min. Four independent measurements were performed for each treatment condition.

### 2.4.7 Statistical Analysis

Statistical differences between results were determined by one-way ANOVA followed by Fisher's LSD test for multiple comparisons with a significance level $p \leq 0.05$ using OriginPro 9.1 software (OriginLab, USA). All the results are expressed as the mean ± standard deviation unless otherwise specified.

## 3. Results and discussion

### 3.1. Cooling temperature profile (CTP)

The formation process of the oleogels within cylindrical containers took place by heat exchange between the hot mixture and the ambient air at AT = 5, 17.5, or 30 °C. During the cooling process, the temperature of the mixture was measured as a function of time. The results are shown in Fig. 1. As it can be observed (especially in the inset), all the samples experienced a non-constant cooling rate with the highest rates in the early stages of the process (until ~25 min). After that, the cooling rate decreased as the temperature was getting closer to AT. As it was expected, samples cooled at the lowest AT (5 °C) developed the highest cooling rates. Although Newton's Law of Cooling can describe the behaviors shown in Fig. 1, this mathematical equation could not be introduced in the equipment programming used in this work. As consequence, each CTP was described as the sum of different linear behaviors as it was mentioned in Section 2.3.

### 3.2. Rheological and image monitoring of gelation process

Fig. 2A and 2B contain polarized images recorded during oleogel formation and the related viscoelastic moduli (G' and G'') for each CTP, respectively. At the first stage of

the cooling process, only one homogeneous phase corresponding to the blend of the molten components was visualized. Subsequently, and with the decrease of temperature it was possible to observe the appearance of the first nuclei of crystals and their fast growth. Network formation seemed to be initiated by sporadic nucleation followed by crystal growth and successive branching. Independently of the CTP, the formation of monoglycerides crystals composing the network occurred between 55 and 46 °C. This suggests that the crystals formation temperature range was determined by the chemical composition of the mixtures. Despite this fact, significant morphological differences in the distribution and size of crystals and aggregates between the different oleogel samples were observed. It can be attributed to the way those temperatures were reached. For a given temperature, it was evident the presence of more connected aggregates of smaller crystals as AT decreased.  In a recent work, Lupi et al. (2016) applied RM as a complementary technique to observe differences in the network structures of MG organogels produced using different oils. Although the images shown by the authors corresponded to oleogels formulated with a lower amount of MG (3% vs. 10% in the present work) and a vegetable oil different to HOSO, it was possible to find a certain visual similarity between those crystal shapes and the ones shown in Fig 2.A (see discussion below).

As it can be noted from Fig 2.A, the major change in the viscoelastic moduli took place during the temperature range in which the crystalline network was being formed. Subsequent increases were not accompanied by detectable morphological changes in the images of the structures indicating that the rheometer would be able to detect a reorganization that had place in another structure scale. The gelation temperatures, determined by multiwave rheological test, resulted to be frequency-independent (data not shown). These temperatures were similar for all samples and ranged between 61 and 64 °C, which means that the gelation point was not affected by the CTP.

Related to the final structure of the obtained oleogels, it was found that micrographs acquired with RM, CLSM, and PLM for a same oleogel sample revealed a strong consistency (Fig. 3). The effect of the CTP on network structure can be visually evidenced. Generally speaking, monoglycerides crystals appeared distributed in irregular, elongated, fibrillar or needle-like shape. Similar MG crystal shapes were reported by Lopez-Martinez et al. (2014) and by Lupi et al. (2016) in oleogels formulated with MG/safflower oil and MG/olive oil, respectively. However, as the AT increased large crystals that formed largest and less branched clusters were observed. Micrographs provided by the CLSM showed a densely packed network of crystals in the oleogel produced at the lowest AT and a more open mesh for the remaining oleogels. Likewise, PLM, indicated that the main difference between samples is the

crystals and clusters size, which was demonstrated by particle size measurements. The significance of all results mentioned in this section is further elaborated upon during the presentation and discussion of the different microscopic and macroscopic parameters.

### 3.3. Microstructural analysis

Micrographs corresponding to the final structure of the oleogels obtained with RM, CLSM, and PLM were used to characterize the formed networks in a more systematic way by different analysis tools using ImageJ software. Table 1 summarizes, among others, the results obtained from the crystal size distribution analysis. As can be noted, the D50 values determined with the three kinds of images of the oleogel samples obtained from a same CTP were very similar. Based on this similarity, it was possible to calculate an average D50 value for each CTP of 35.68 ± 2.18, 57.18 ± 0.85, and 70.30 ± 1.08 um for 5, 17.5 and 30 °C respectively. Significant differences (p < 0.05) were found between these values indicating that the crystal length D50 decreased with the decrease in AT value. This result corroborates the generally admitted relation between the cooling rate and its associated crystal size. On the other hand, a slightly high average span value was obtained at CTP corresponding to 5 °C, indicating a wider size distribution. Although it was not found in the literature comparative data for MG crystals sizes, it has been reported that the mean crystal length of rice bran wax (RBX) in oleogels (5% wt of RBX) obtained under static conditions decreased from about 21.0 to 9.8 um when the cooling rate was increased from 1.5 to 5 °C/min (Blake & Marangoni, 2015). The discrepancies between crystals size from this study and those reported values could be explained by the differences in the nature of structurant molecules, used concentrations, and cooling processes.

Furthermore, it was found that PLM and CLSM images of oleogels cooled following the CTP of 5 and 17.5 °C showed similar values of PAF, with averages values ranging between 72.36 and 75.39% , but significantly lower than those obtained at 30 °C. The values acquired from PLM and CLSM image analysis were consistent, whereas processing RM images by auto threshold tool was not possible because of the color similarity between the crystals and the oil. To solve this problem, the Color Inspector 3D plugin was used to determine the crystal area in RM images and the remaining area corresponded to PAF%. In this case, no significant differences between the used CTP were detected, being the average PAF 13.02%. The obtained values resulted much smaller than those previously determined with PLM and CLSM. The differences found in results obtained by applying different techniques to characterize the crystal network could be attributed to the fact that PLM and CLSM images were achieved from samples removed from the rheometer plate, whereas the RM images were directly

captured during the oleogel formation. The careful removal of the oleogel from the rheometer plate allowed us to keep intact the crystal structure but probably not the oil distribution, which was affected by the preparation of the sample to its observation. Thus, based on RM images which were taken in situ, it was possible to conclude that the area occupied by crystals and oil did not depend on the used CTP. Blake and Marangoni (2015) also reported not having found statistical differences in the PAF of oleogels containing equivalent concentration of waxes both slowly cooled and rapidly cooled. From these results, the superiority of using an in situ method such as RM to obtain PAF% can be deduced.

*3.3.1. Fractal dimension: images analysis and weak-link regime for colloidal dispersion*
*Image analysis*. Mean values of the 3D fractal dimension (D) determined by the box counting method on PLM, CLSM, and RM images resulted in the range of 2.74 - 2.89 (Table 1). Some significant differences between D values obtained from images corresponding to different micrograph techniques were detected for different CTP. Images from PLM provided similar D values ($p > 0.05$), independently of the CTP, showing no statistical differences compared with those obtained from CLSM at AT 17.5 and 30°C. However, micrographs from CLSM and RM of oleogels obtained at 5 °C showed slightly higher values of D compared to those corresponding to 17.5 and 30°C.

*Weak-link regime for colloidal dispersion*. As it was explained in the methodology section (2.4.4.2.1), DSC results were used to obtain the reduced crystallinity in order to apply the weak-link regime theory. The thermal profile of samples obtained from DSC measurements showed two exothermic phase transitions, the first one occurring between 59 and 49 °C and the second one, narrower than the former, between 41 and 38 °C. Based on previous works (Chen, Van Damme, & Terentjev, 2008; Ferro et al., 2019; López-Martínez et al., 2014), in which the thermal behavior of MG mixtures of stearic and palmitic acids -with high concentration of stearic acid- in different oils was studied, it was possible to assign the first peak to the crystallization of MG in the inverse lamellar $\alpha$ state and the second one to the transition to sub-$\alpha$ state. When polymorphic transformations are not involved during crystallization of any given compound, it is possible to use the area under the crystallization curve to obtain F values according to Equation 6. Thus, the area of the first peak was processed to obtain F values which were correlated with G' values corresponding to mentioned temperature range for each CTP. The experimental points related to the systems containing a high volume fraction of solids (between 74% and 98%) were adequately fitted with a linear regression ($0.79 < R^2 < 0.99$, data not shown). Fractal dimension values calculated from the slopes resulted about 6% lower than those obtained by image analysis. The statistical analysis also showed significant differences between the

D values obtained for different CTP. This methodology, as well as RM and CLSM images analysis, revealed that the applied CTP had an effect on this microstructural parameter, being the highest values those that correspond to oleogels obtained at AT = 5 °C. This means that more ordered crystal networks took place due to the presence of homogeneous small crystals (at the lowest AT), leading to a better spatial mass distribution. Ojijo et al. (2004) determined the fractal dimension of olive oil/MG network aggregates using the G' value at 25 °C of oleogels prepared with different MG proportions reporting a value of 2.58, which is close to those found in the present contribution.

*3.3.2 Parameters of the modified Avrami model*

Fig. 4 shows the evolution over time of the cumulative crystal mass present in oleogels. It can be seen that all these curves show similar sigmoidal shapes. This means the presence of an initial time period during which MG are not crystallized, corresponding to the completely molten sample, followed by a period of rapid crystallization. That initial period of time increased with AT. Whatever the CTP, the modified Avrami model succeeded in describing the experimental points properly ($R^2$>0.96). The fitting parameters, $t_0$ and $k_{app}$, depended on AT (Table 2). As it was expected, the highest $t_0$ and the lowest $k_{app}$ values were obtained at the highest AT indicating that crystallization started later and proceeded more slowly at lower cooling rate. On the other hand, the Avrami index resulted close to 2 independently of the CTP. This resemblance between values indicated that the nucleation and the crystal growth mechanism took place in a similar way. Since RM images would indicate that crystallization was conducted by sporadic nucleation, an *n* value of 2 would be associated with a crystal growth in needle-like form (1D), which was in agreement with the shape of crystals showed by images. It is worth mentioning that the local cooling rates corresponding to the crystallization process times for used CTP ranged between 1.2 and 2.4 °C/min. Meng et al. (2014) reported that the crystal growth of MG was a rod-like growth of instantaneous nuclei at higher degree of supercooling when they studied the crystallization by pulsed nuclear magnetic resonance. A possible explanation for this difference in the type of nucleation found might be that the authors evaluated cooling rates higher than this work, in which the crystallization processes were initiated and completed in less than 1 min. In fact, a more instantaneous nucleation process has been associated with a shorter induction time (Meng et al., 2014). On the other hand, a noticeable finding was that although all the CTP assayed led to a similar crystallization mechanism, the change of cooling rates generated crystals with different sizes. As a result of the highest cooling rate, the network was formed by smaller and more numerous crystals.

Another approach to study the dynamics of the crystalline network formation was applied based on the change of complex viscosity of oleogels during gelation. Fig. 5.A shows representative curves of η* for each CTP. Since η* values are related to G' and G" data, it is possible to note a similar behavior between these curves and those shown in Fig. 2. However, changes of curvature of η* curves (inflection points) were more clearly distinguishable in the results obtained by the conventional rheometer. Points shown in Fig. 5.B were obtained using the Equation (3) with $\eta^*_{max}$ defined as the maximum value of sample complex viscosity acquired during the entire cooling process (global analysis). In this case, since multiple combinations of parameter values led to adequate points adjusts, the value of $t_0$ was determined by extrapolating $Y/Y_{max}$ to 0 using the initial increase in that variable. Best-fit lines are also included in the mentioned figure, and the corresponding parameter values of the modified Avrami model are reported in Table 2. As it can be noted, the curves for 5 and 17.5 °C also showed a sigmoidal shape but differed from the previous ones obtained by image analysis. Moreover, the behavior of the curve corresponding to 30 °C could not be well represented by the selected model. With the assumption that the evolution of η* could be caused only by the crystal formation, the duration of crystallization process would result longer than those indicated by RM images. For example, when the cooling process was conducted at AT = 5 °C, the time period determined for crystallization from rheological measurements was about 17 min whereas the obtained with RM images was about 3.5 min. Besides that, the induction times were higher for all the CTP and ranged between 10 and 14 min. These results were in agreement with those obtained by Ho Lam and Rogers (2011), who indicated that the G', and therefore the η*, is not only a function of the change in phase volume, but also of other system variables such as the spatial distribution of mass, crystal size, and inter-crystal interactions. In this way, obtained $n$ values, which ranged between 0.96 and 1.49 could not be directly related to the nucleation and growth dimension of crystals. On the other hand, because of the highest $k_{app}$ values were obtained for AT = 5 °C and taking into account the previous results obtained in the fractal dimension analysis, this could suggest that $k_{app}$ parameter would be closely associated with the spatial distribution of crystal mass in the oleogels.

Next, it was considered the possibility of finding appropriate $n$ values using rheological data referred only to the times in which crystals formation was observed by RM images. Thus, an additional analysis was conducted using the Equation (3) with $\eta^*_{max}$ defined as the maximum value of sample complex viscosity recorded until around 47 °C. This point corresponded to the inflection of η* curves. Therefore, data transformed to $Y/Y_{max}$ vs. time and their fitting by the modified Avrami model are shown in Fig. 5.C.

Using this approach, the behavior of the points for each CTP could be appropriately described by the selected equation ($R^2$>0.98). Induction times increased with increasing of AT. The *n* index values were close to 2, the expected value, for all CTP. Furthermore, $k_{app}$ value resulted lower at 30 than 17.5 and 5°C, showing the same AT dependence but lower values than the ones obtained from RM images analysis.

As Table 2 shows, differences were found between the induction times determined for each type of analysis at one specific AT. Values of $t_0$ obtained by image analysis resulted slightly higher than those experimental times in which it was possible to visually detect crystals formation. It is important to mention that other adjusts were performed setting $t_0$ equal to these experimental values, but the associated parameter *n* resulted in values without adequate physical meaning. On the other hand, $t_0$ values obtained by global analysis of η* would be related to the entire process of oleogel formation. Moreover, these times exceeded the period required for MG crystallization according to the findings by image analysis. The last approach based on the evolution of η* values for a limited time domain led to the lowest $t_0$ values, which could indicate a greater sensibility of this type of analysis.

The most important findings to emerge from these results was that RM images analysis of crystalline systems can be used to successfully determine the Avrami index. In addition, we found that it would be possible to apply the modified Avrami model to characterize microstructures using rheology when it is known the range of temperatures in which the crystals formation occurred, information that could be obtained by RM images or DSC, for instance. While this approach requires that its applicability be tested in other systems beyond of MG, this finding represents an improvement with respect to the lack of accurately reported for Ho Lam and Rogers (2011) in the use of rheology to determine the kinetics of crystallization of 12-hydroxy stearic acid, stearic acid, and trihydroxystearin.

### 3.4. Macroscopic properties

Some of the most important macroscopic properties of produced oleogels are shown in Table 3. The elastic modulus of the resulting oleogels ranged between around 3.6 $\times10^5$ and 1.9 $\times10^6$ Pa and the ratio G''/G' resulted lower than 0.1 (data not shown) which would indicate that MG used in 10 wt% would be able to form strong gels (Patel, Babaahmadi, Lesaffer, & Dewettinck, 2015). Statistically, more elastic materials were produced using CTP of 30 > 17.5 > 5 °C. A similar effect was reported by Ojijo et al. (2004) but using constant rates of cooling (between 0.42 and 1.49 °C/min) in the rheometer. In order to link microscopic and macroscopic behavior, values of G' and fractal dimension were plotted as an AT function (graph not shown). Since it was not found a clear trend between G' and D values, it is possible to think that other factors

like interaction forces, size and order of crystals are affecting the response to small deformation rheology.

The oleogels obtained under different CTP showed OBC values higher than 78%, which indicates that MG crystal networks provided high levels of structuration and oil stabilization. According to the p-value, significant differences were found in OBC due to the AT. The maximum OBC value was reached at 5 °C and this value decreased with the increase in AT. Since that lowest temperature produced a network of homogeneous small crystals, this provided a greater surface area and a more tortuous pathway impeding the migration and consequent leak of oil. A similar result was found by Blake and Marangoni (2015) studying the effect of cooling rate on wax oleogels. This result can also be correlated with the fractal dimension since the oleogels with highest D showed the highest OBC value. This finding was consistent with those reported by Blake et al. (2014) who investigated the relationship between microstructure and OBC of wax oleogels. Authors suggested that, as the solid mass is more evenly distributed through the material, the oil present in the material is more strongly bound. On the other hand, it was not possible to establish a relationship between OBC and PAF% values determined by analysis of RM, as could have been expected, due to PAF% did not show AT dependence. PAF% parameter refers to the total amount of free oil present in the visualized sample but not the way in which it is distributed across the crystal network, being this aspect the determining factor in the ability to retain oil. It allows to think about the determination of the size of pores as a better estimate parameter to find a relationship between OBC and image analysis.

As can been seen from Table 3, hardness values changed significantly with the used CTP. The lowest cooling rate process (higher AT) allowed to obtain a material with a hardness value up to 39% greater despite having the same composition. Results would indicate that aggregates of longer crystals provided a greater resistance to the first penetration. Generally, plastic fat networks with bigger crystal structures tend to be softer than those with small sized crystals at the same solids content (Ojijo, Kesselman, et al., 2004; Wright, Scanlon, Hartel, & Marangoni, 2001). Our results obtained from penetration TPA test differed from these previous studies, but they were consistent with those reported for similar monoglycerides oleogels systems (Giacomozzi et al., 2018; Palla et al., 2017), in which the hardest materials were achieved using cooling temperatures higher than 5 °C ( i.e. the temperature that produced the smallest crystals). A possible explanation for these results may be related to the nature of the TPA test together with the features of the studied materials. The effect of CTP on the penetration work values corresponding to the first penetration cycle (WP1) was the same than the showed for hardness values, being the WP1

values of 23.46 ± 1.43, 21.62 ± 1.14, and 25.52 ± 1.23 Pa.s for 5, 17.5, and 30 °C, respectively. However, the penetration work values in the second cycle (WP2) showed an opposite behavior. The determined WP2 values were 6.46 ± 0.38, 4.20 ± 0.16, and 2.09 ± 0.21 Pa.s for 5, 17.5, and 30 °C, respectively. Since WP2 provides information about the unbroken structures after the first penetration cycle and therefore about the presence of more persistent bonds, it can be thought that, finally, oleogels with a network comprised of smaller crystals proved to be more large-deformation resistant. Thus, although the trend found in the hardness values of the oleogels could not be correlated with the trend found in the D values, it was possible to find a positive correlation between the highest WP2 and the highest D.

As far as we know, this study is the first to search for a relationship between the fractal dimension of crystalline networks of oleogels and their mechanical properties. Narine and Marangoni (1999b) found a direct relationship between D and hardness index of other fat systems (milkfat, cocoa butter, palm oil, lard, and tallow). The authors highlight that the fact that the fractal dimension acts as an indicator of hardness is invaluable to the food industry in which the development of fat systems with specific hardness is required. Since the use of RM image analysis allowed to obtain accurate measurements of fractal dimensions with reduced time and effort compared to the weak-link regime approach, a more in-depth research would be required in order to explore the potential of using this technique to obtain D values in different fat materials that could then be related with their hardness or, failing that, with the penetration work of the second cycle.

## 4. Conclusions

In this study, we analyzed the effect of using non-constant cooling rates on the crystallization and gelation processes of MG oleogels and therefore on their final properties. In conclusion, the CTP affected both formation and properties of the oleogels. Although crystal formation took place during a similar range of temperatures, it was observed significant morphological differences in the distribution and size of crystals and aggregates between the different oleogel samples. An oleogel network structure with smaller crystals and more branched clusters was obtained when the lowest ambient temperature AT (higher cooling rates) was used. Micrographs obtained from RM, CLSM, and PLM revealed a strong consistency in the size of the crystals. Furthermore, since RM were acquired in situ, it provided valuable information related to network structures. Analysis of these images revealed that the area occupied by crystals and oil did not depend on used CTP. Moreover, it was possible to obtain kinetics of crystallization which were adjusted successfully by the modified Avrami

model. Additionally, another of the most significant findings to emerge from this study was that RM images were also useful to obtain a more restricted time domain in which rheological data could be used to find values of Avrami index that seems to be related only to the crystallization process.

The analysis of RM images turned out to be an efficient approach to obtain accurate measurement of the fractal dimension. Furthermore, the results obtained by RM images analysis and the weak-link regime approach applied to dynamic systems were very similar. This allows us to affirm that the weak-link regime approach was appropriate to describe the relationship between G' and crystal formation during the obtention of MG oleogels. Likewise, it was found that higher values of fractal dimension were associated with gels exhibiting a greater number of homogeneous small crystals. These oleogels showed the highest capacity to retain oil and were more resistant to deformation during the second penetration cycle in the TPA assay.

Based on results obtained in this work it is possible to conclude that rheo-microscopy represented a valuable tool to interrogate the structural characteristics of the MG oleogels obtained under different CTP. Besides that, the insights gained from this study may be of assistance to the food industry who required a better understanding of the oleogelation process that allows it to control the quality of obtained oleogels, which could be utilized to replace the *trans* and saturated fats in food formulations.

**References**

Agregán, R., Barba, F. J., Gavahian, M., Franco, D., Khaneghah, A. M., Carballo, J., … Lorenzo, J. M. (2019). Fucus vesiculosus extracts as natural antioxidants for improvement of physicochemical properties and shelf life of pork patties formulated with oleogels. *Journal of the Science of Food and Agriculture*, (December 2018). https://doi.org/10.1002/jsfa.9694

Allen, T. (1997). Particle size by image analysis. In *Particle Size Measurement Volume 1 Powder sampling and particle size measurement* (Fifth edit). London, UK: Chapman & Ball.

AOCS. (2009). *Official methods and recommended practices of the American Oil Chemists' Society.* Champaign, USA.

Barthel, K. U. (2004). Color Inspector 3D. Retrieved July 2, 2019, from http://rsb.info.nih.gov/ij/plugins/color-inspector.html

Blake, A. I., Co, E. D., & Marangoni, A. G. (2014). Structure and physical properties of plant wax crystal networks and their relationship to oil binding capacity. *JAOCS, Journal of the American Oil Chemists' Society*, *91*(6), 885–903. https://doi.org/10.1007/s11746-014-2435-0

Blake, A. I., & Marangoni, A. G. (2015). The Effect of Shear on the Microstructure and Oil Binding Capacity of Wax Crystal Networks. *Food Biophysics*, *10*(4), 403–415. https://doi.org/10.1007/s11483-015-9398-z

Chen, C. H., & Terentjev, E. M. (2009). Aging and metastability of monoglycerides in hydrophobic solutions. *Langmuir*, *25*(12), 6717–6724. https://doi.org/10.1021/la9002065

Chen, C. H., Van Damme, I., & Terentjev, E. M. (2008). Phase behavior of C18 monoglyceride in hydrophobic solutions, 432–439. https://doi.org/10.1039/b813216j

da Pieve, S., Calligaris, S., Co, E., Nicoli, M. C., & Marangoni, A. G. (2010). Shear Nanostructuring of monoglyceride organogels. *Food Biophysics*, *5*(3), 211–217. https://doi.org/10.1007/s11483-010-9162-3

Dassanayake, L. S. K., Kodali, D. R., & Ueno, S. (2011). Formation of oleogels based on edible lipid materials. *Current Opinion in Colloid and Interface Science*, *16*(5), 432–439. https://doi.org/10.1016/j.cocis.2011.05.005

Dàvila, E., & Parés, D. (2007). Structure of heat-induced plasma protein gels studied by fractal and lacunarity analysis. *Food Hydrocolloids*, *21*(2), 147–153. https://doi.org/10.1016/j.foodhyd.2006.02.004

Dhaka, V., & Gulia, N. (2011). Trans fats — sources , health risks and alternative approach - A review, *48*(October), 534–541. https://doi.org/10.1007/s13197-010-0225-8

Doan, C. D., Tavernier, I., Okuro, P. K., & Dewettinck, K. (2018). Internal and external factors affecting the crystallization, gelation and applicability of wax-based oleogels in food industry. *Innovative Food Science and Emerging Technologies*, *45*(August 2017), 42–52. https://doi.org/10.1016/j.ifset.2017.09.023

Fayaz, G., Goli, S. A. H., Kadivar, M., Valoppi, F., Barba, L., Calligaris, S., & Nicoli, M. C. (2017). Potential application of pomegranate seed oil oleogels based on monoglycerides, beeswax and propolis wax as partial substitutes of palm oil in functional chocolate spread. *LWT - Food Science and Technology*, *86*, 523–529. https://doi.org/10.1016/j.lwt.2017.08.036

Ferro, A. C., Okuro, P. K., Badan, A. P., & Cunha, R. L. (2019). Role of the oil on glyceryl monostearate based oleogels. *Food Research International*, *120*(November 2018), 610–619. https://doi.org/10.1016/j.foodres.2018.11.013

Gaudino, N., Ghazani, S. M., Clark, S., Marangoni, A. G., & Acevedo, N. C. (2019). Development of lecithin and stearic acid based oleogels and oleogel emulsions for edible semisolid applications. *Food Research International*, *116*(September 2018), 79–89. https://doi.org/10.1016/j.foodres.2018.12.021

Gavahian, M., Tiwari, B. K., Chu, Y., Ting, Y., & Farahnaky, A. (2019). Food texture as affected by ohmic heating: Mechanisms involved, recent findings, benefits, and limitations. *Trends in Food Science & Technology*, *86*, 328–339. https://doi.org/10.1016/j.tifs.2019.02.022

Giacomozzi, A. S., Carrín, M. E., & Palla, C. A. (2018). Muffins Elaborated with Optimized Monoglycerides Oleogels: From Solid Fat Replacer Obtention to Product Quality Evaluation. *Journal of Food Science*, 1–11. https://doi.org/10.1111/1750-3841.14174

Ho Lam, R. S., & Rogers, M. A. (2011). Experimental validation of the modified Avrami model for non-isothermal crystallization conditions. *CrystEngComm*, *13*(3), 866–875. https://doi.org/10.1039/C0CE00523A

HORIBA Scientific. (2010). a Guidebook To Particle Size Analysis. Retrieved July 2,
   2019, from
   https://www.horiba.com/fileadmin/uploads/Scientific/eMag/PSA/Guidebook/pdf/PS
   A_Guidebook.pdf

Hughes, N. E., Marangoni, A. G., Wright, A. J., Rogers, M. A., & Rush, J. W. E. (2009).
   Potential food applications of edible oil organogels. *Trends in Food Science and
   Technology*, *20*(10), 470–480. https://doi.org/10.1016/j.tifs.2009.06.002

Karperien, A. (2004). FracLac for ImageJ. FracLac Advanced User's Manual. Retrieved
   July 2, 2019, from https://imagej.nih.gov/ij/plugins/fraclac/fraclac-manual.pdf

Liu, X. Y., & Sawant, P. D. (2001). Formation kinetics of fractal nanofiber networks in
   organogels. *Applied Physics Letters*, *79*(21), 3518–3520.
   https://doi.org/10.1063/1.1415609

López-Martínez, A., Morales-Rueda, J. A., Dibildox-Alvarado, E., Charó-Alonso, M. A.,
   Marangoni, A. G., & Toro-Vazquez, J. F. (2014). Comparing the crystallization and
   rheological behavior of organogels developed by pure and commercial
   monoglycerides in vegetable oil. *Food Research International*, *64*, 946–957.
   https://doi.org/10.1016/j.foodres.2014.08.029

Lupi, F. R., Greco, V., Baldino, N., de Cindio, B., Fischer, P., & Gabriele, D. (2016).
   The effects of intermolecular interactions on the physical properties of organogels
   in edible oils. *Journal of Colloid and Interface Science*, *483*, 154–164.
   https://doi.org/10.1016/j.jcis.2016.08.009

Meng, Z., Yang, L., Geng, W., Yao, Y., Wang, X., & Liu, Y. (2014). Kinetic study on the
   isothermal and nonisothermal crystallization of monoglyceride organogels. *The
   Scientific World Journal*, *2014*. https://doi.org/10.1155/2014/149753

Mert, B., & Demirkesen, I. (2016). Evaluation of highly unsaturated oleogels as
   shortening replacer in a short dough product. *LWT - Food Science and
   Technology*, *68*, 477–484. https://doi.org/10.1016/j.lwt.2015.12.063

Narine, S. S., & Marangoni, A. G. (1999a). Fractal nature of fat crystal networks.
   *Physical Review E - Statistical Physics, Plasmas, Fluids, and Related
   Interdisciplinary Topics*, *59*(2), 1908–1920.
   https://doi.org/10.1103/PhysRevE.59.1908

Narine, S. S., & Marangoni, A. G. (1999b). Relating structure of fat crystal networks to

mechanical properties: A review. *Food Research International*, *32*(4), 227–248. https://doi.org/10.1016/S0963-9969(99)00078-2

O'Sullivan, C. M., Barbut, S., & Marangoni, A. G. (2016). Edible oleogels for the oral delivery of lipid soluble molecules: Composition and structural design considerations. *Trends in Food Science and Technology*, *57*, 59–73. https://doi.org/10.1016/j.tifs.2016.08.018

Ojijo, N. K. O., Kesselman, E., Shuster, V., Eichler, S., Eger, S., Neeman, I., & Shimoni, E. (2004). Changes in microstructural, thermal, and rheological properties of olive oil/monoglyceride networks during storage. *Food Research International*, *37*(4), 385–393. https://doi.org/10.1016/j.foodres.2004.02.003

Ojijo, N. K. O., Neeman, I., Eger, S., & Shimoni, E. (2004). Effects of monoglyceride content, cooling rate and shear on the rheological properties of olive oil/monoglyceride gel networks. *Journal of the Science of Food and Agriculture*, *84*(12), 1585–1593. https://doi.org/10.1002/jsfa.1831

Palla, C., Giacomozzi, A., Genovese, D. B., & Carrín, M. E. (2017). Multi–objective optimization of high oleic sunflower oil and monoglycerides oleogels: Searching for rheological and textural properties similar to margarine. *Food Structure*, *12*. https://doi.org/10.1016/j.foostr.2017.02.005

Patel, A. R., Babaahmadi, M., Lesaffer, A., & Dewettinck, K. (2015). Rheological Profiling of Organogels Prepared at Critical Gelling Concentrations of Natural Waxes in a Triacylglycerol Solvent. *Journal of Agricultural and Food Chemistry*, *63*(19), 4862–4869. https://doi.org/10.1021/acs.jafc.5b01548

Rocha-Amador, O. G., Gallegos-Infante, J. A., Huang, Q., Rocha-Guzman, N. E., Rociomoreno-Jimenez, M., & Gonzalez-Laredo, R. F. (2014). Influence of commercial saturated monoglyceride, mono-/diglycerides mixtures, vegetable oil, stirring, and temperature on the physical properties of organogels. *International Journal of Food Science*, *2014*. https://doi.org/10.1155/2014/513641

Rogers, M. A., & Marangoni, A. G. (2008). Non-isothermal nucleation and crystallization of 12-hydroxystearic acid in vegetable oils. *Crystal Growth and Design*, *8*(12), 4596–4601. https://doi.org/10.1021/cg8008927

Rogers, M. A., Tang, D., Company, T. H., & Marangoni, A. G. (2008). *Fat Crystal Networks*. https://doi.org/10.1007/978-0-387-71947-4

Shahrivar, K., & de Vicente, J. (2014). Thermogelling magnetorheological fluids. *Smart Materials and Structures*, *23*(2). https://doi.org/10.1088/0964-1726/23/2/025012

Singh, A., Auzanneau, F. I., & Rogers, M. A. (2017). Advances in edible oleogel technologies – A decade in review. *Food Research International*, *97*, 307–317. https://doi.org/10.1016/j.foodres.2017.04.022

Souza, R. J. De, Mente, A., Maroleanu, A., Cozma, A. I., Ha, V., Kishibe, T., … Anand, S. S. (2015). Intake of saturated and trans unsaturated fatty acids and risk of all cause mortality , cardiovascular disease , and type 2 diabetes : systematic review and meta-analysis of observational studies, 1–16. https://doi.org/10.1136/bmj.h3978

Toro-Vazquez, J. F., Dibildox-Alvarado, E., Charó-Alonso, M., Herrera-Coronado, V., & Gómez-Aldapa, C. A. (2002). The Avrami index and the fractal dimension in vegetable oil crystallization. *JAOCS, Journal of the American Oil Chemists' Society*, *79*(9), 855–866. https://doi.org/10.1007/s11746-002-0570-y

Wright, a. J., Scanlon, M. G., Hartel, R. W., & Marangoni, a. G. (2001). Rheological Properties of Milkfat and Butter Concise Reviews in Food Science. *Journal of Food Science*, *66*(8), 1056–1071. https://doi.org/10.1111/j.1365-2621.2001.tb16082.x
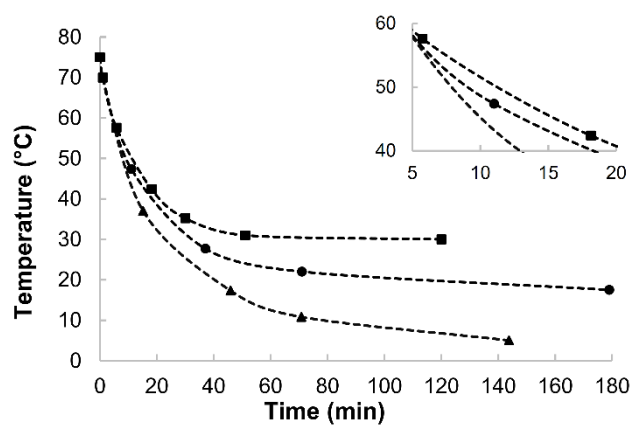
Fig. 1. Temperature profile showed by oleogel mixtures cooled at ambient temperature (AT) of 5 (▲), 17.5 (●) and 30 °C (■). Dotted lines represent the sample temperature trend.
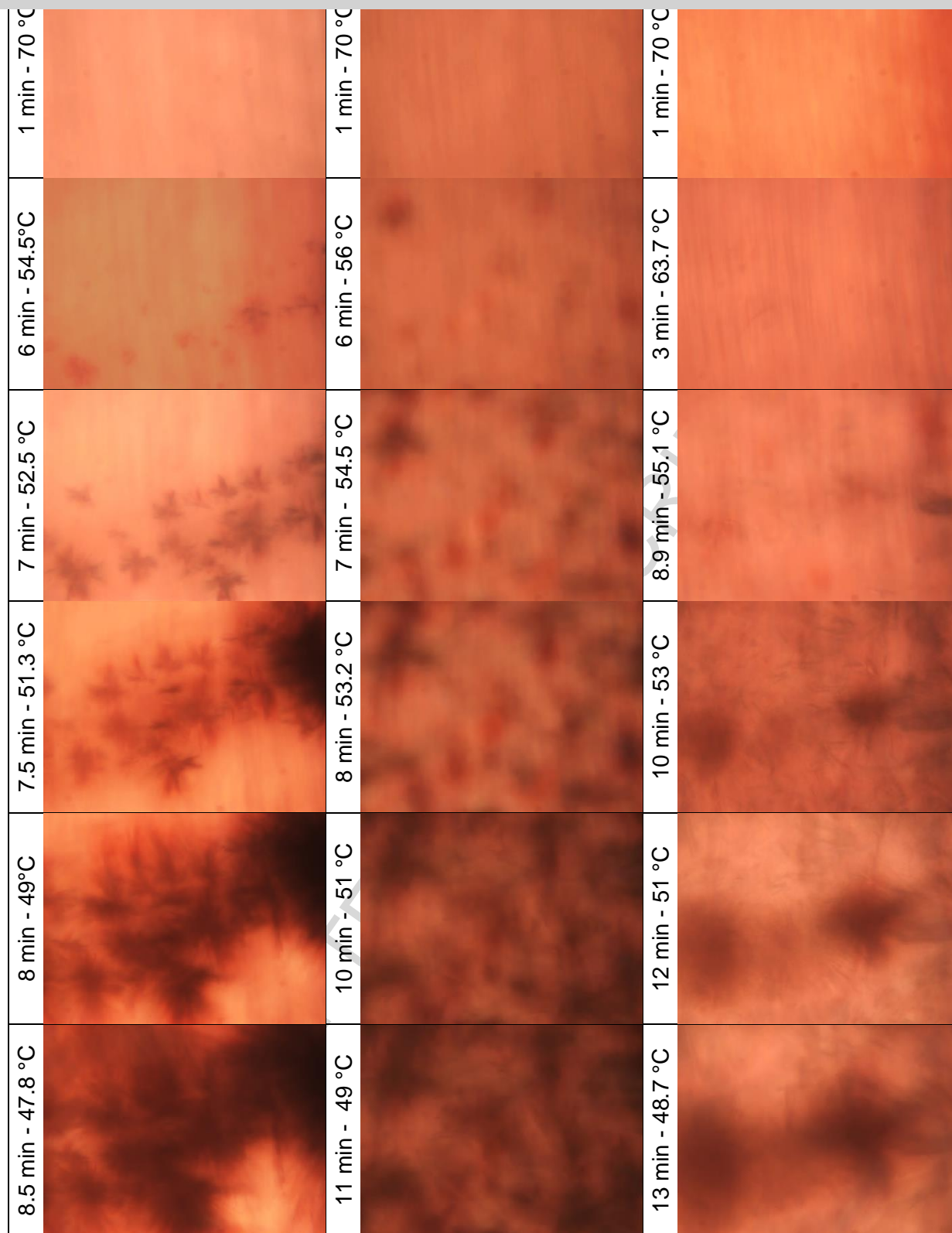
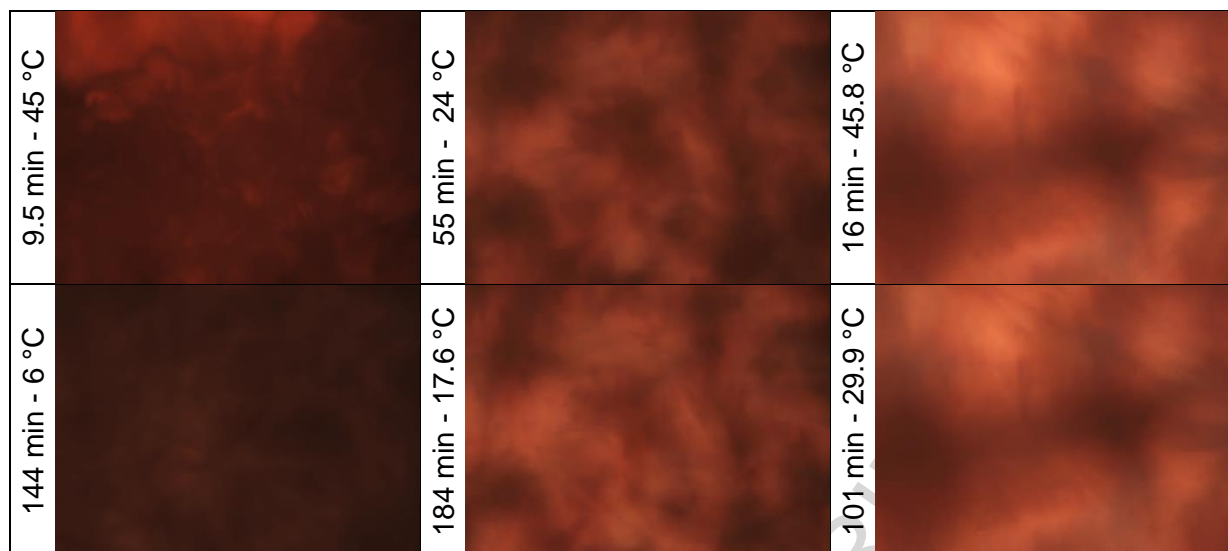|  | 5 °C | 17.5 °C | 30 °C |
|--|------|---------|-------|
| | 1 min - 70 °C | 1 min - 70 °C | 1 min - 70 °C |
| | 6 min - 54.5°C | 6 min - 56 °C | 3 min - 63.7 °C |
| | 7 min - 52.5 °C | 7 min - 54.5 °C | 8.9 min - 55.1 °C |
| | 7.5 min - 51.3 °C | 8 min - 53.2 °C | 10 min - 53 °C |
| | 8 min - 49°C | 10 min - 51 °C | 12 min - 51 °C |
| | 8.5 min - 47.8 °C | 11 min - 49 °C | 13 min - 48.7 °C |

Fig. 2.A. Rheo-microscope images recorded during oleogel formation process using the cooling temperature profile (CTP) corresponding to AT of 5, 17.5, and 30 °C.
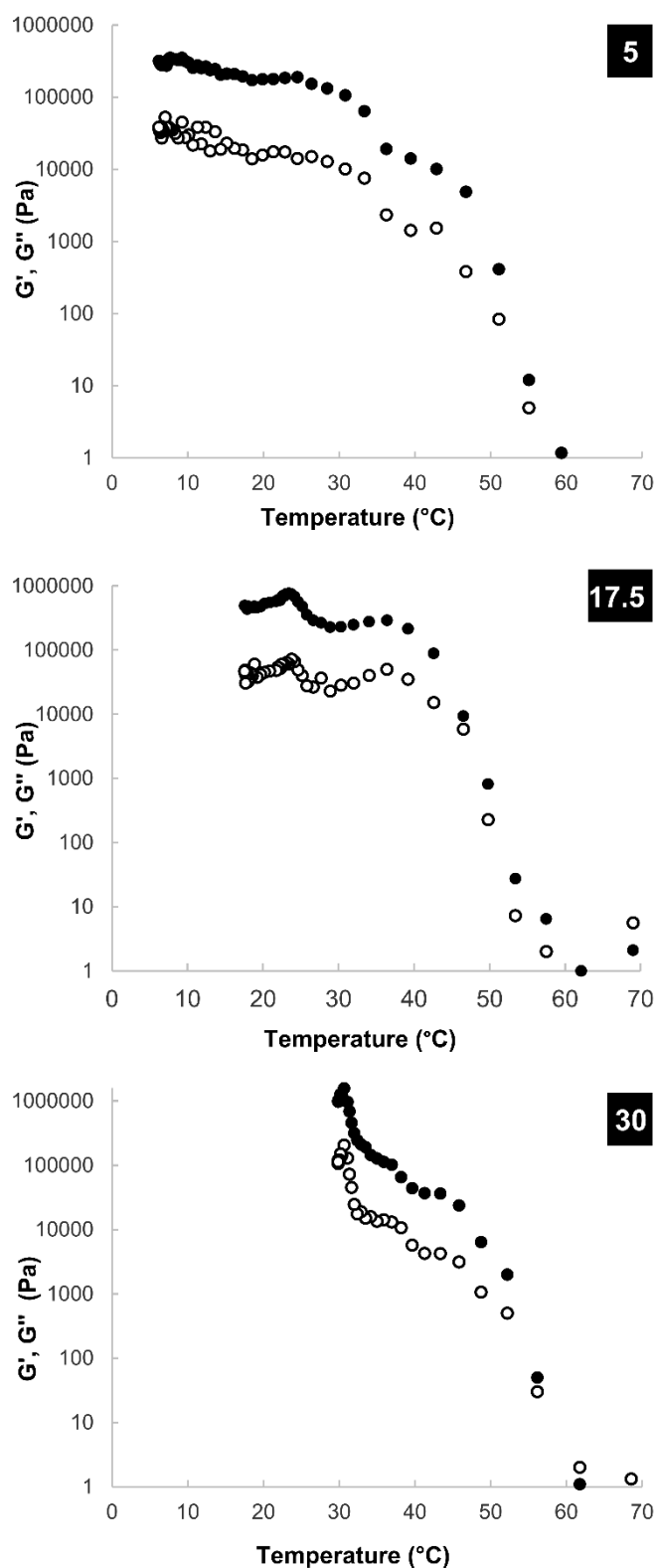
Fig. 2.B. G' (●) and G" (○) values recorded simultaneously with rheo-microscope images (Fig. 2.A) during oleogel formation process using the CTP corresponding to AT of 5, 17.5, and 30 °C.
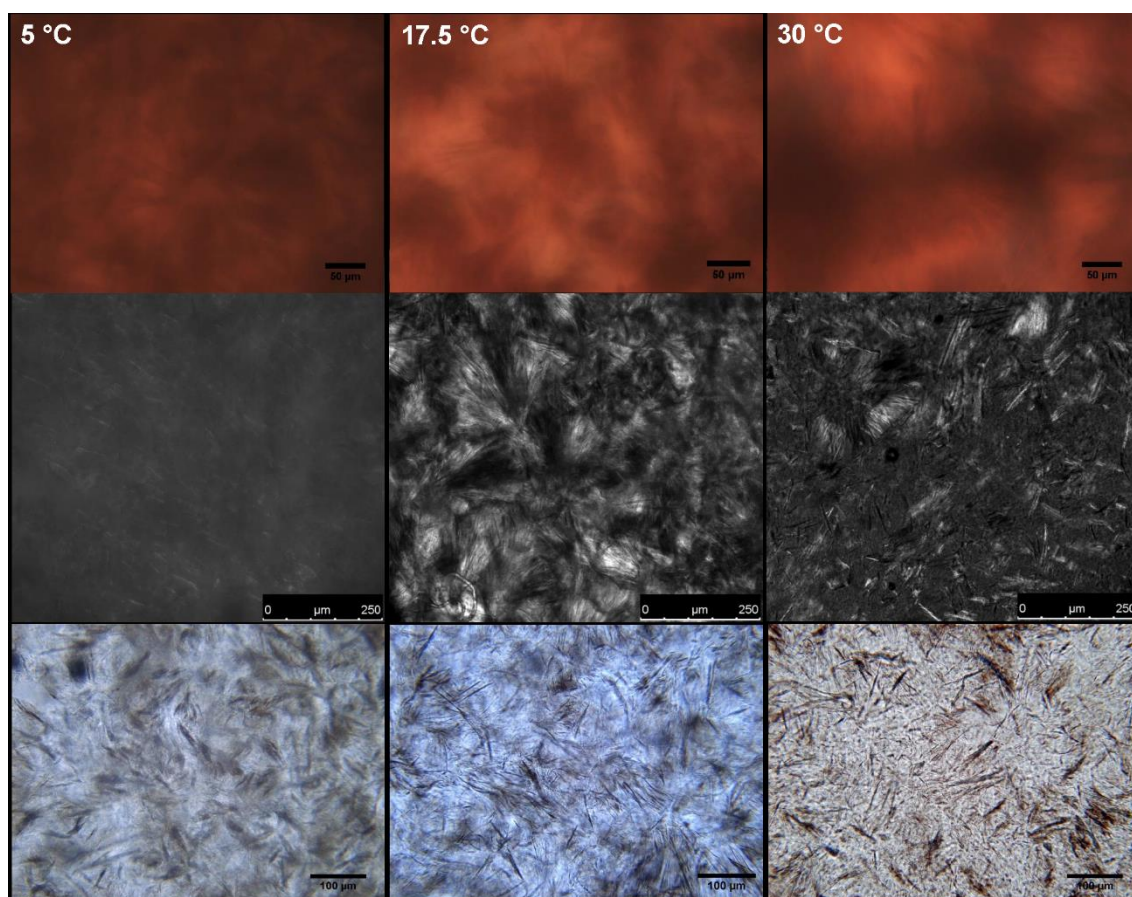
Fig. 3. Images of oleogel final structures visualized using rheo-microscope (top), confocal laser microscope (middle), and polarized light microscope (bottom). The oleogels were obtained using the CTP corresponding to the specified AT.
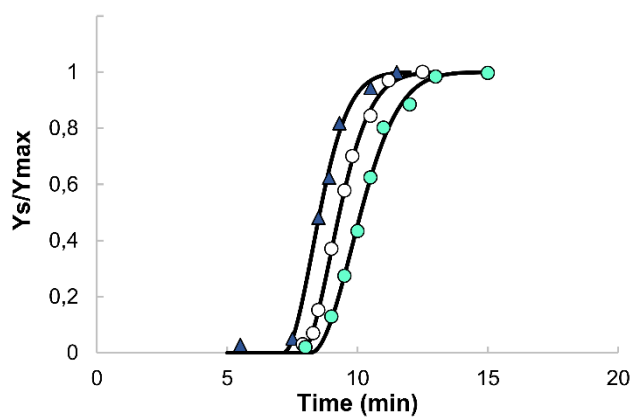
Fig. 4. Time evolution of Ys/Ymax as a function of the crystalline solid material quantified by rheo-microscope images analysis for oleogels obtained using the CTP corresponding to 5 (▲), 17.5 (○) and 30 °C (●). Lines represent the fitted data to the modified Avrami model.
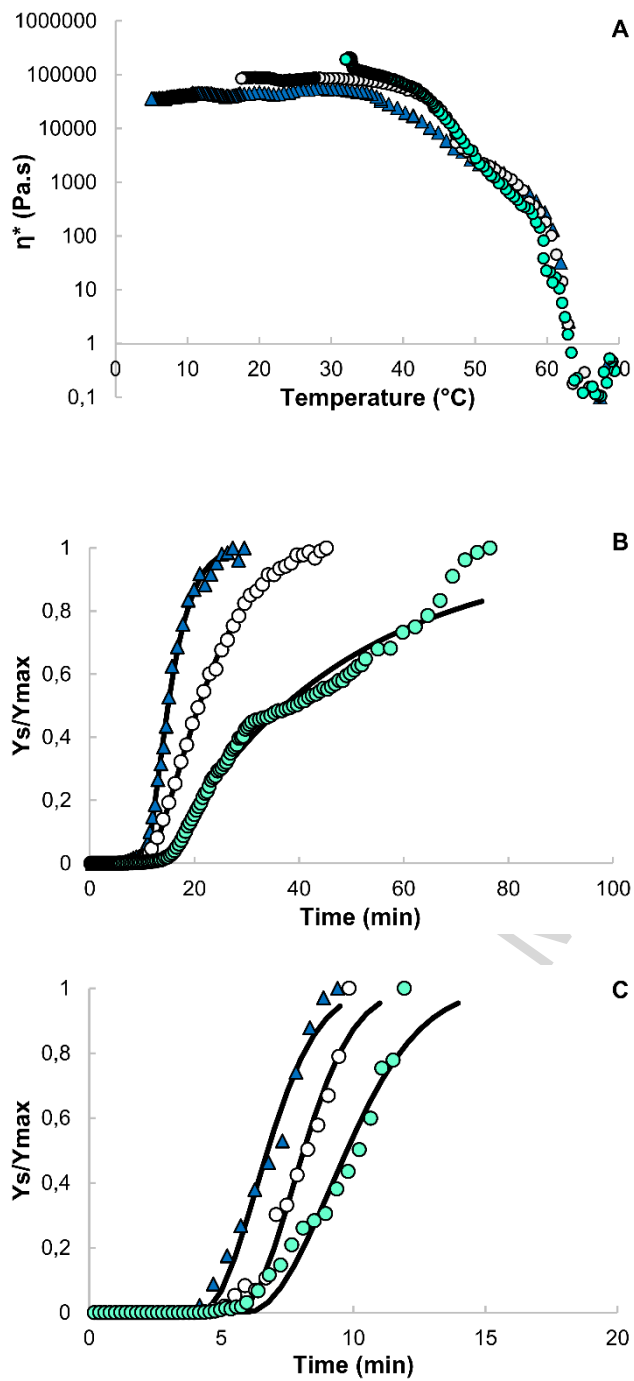
Fig. 5. Evolution of (A) the complex viscosity, η*, of oleogels during cooling at AT of 5 (▲), 17.5 (○), and 30 °C (●), and the corresponding Ys/Ymax obtained as a function of η* by analysis of (B) the cooling global process and (C) the crystals formation stage. Lines represent the fitted data to the modified Avrami model.

**Table 1** Microstructural parameters of MG/HOSO oleogels as a function of the cooling temperature profile (CTP) used for their formation.

| | CTP corresponding to | | | | | |
|---|---|---|---|---|---|---|
| | 5 °C | | 17.5 °C | | 30 °C | |
| | Crystal length | | | | | |
| | D50 (um) | Span | D50 (um) | Span | D50 (um) | Span |
| PLM | 38.19 | 0.52 | 56.22 | 0.45 | 69.40 | 0.51 |
| CLSM | 34.34 | 0.57 | 57.82 | 0.41 | 71.50 | 0.42 |
| RM | 34.50 | 0.53 | 57.50 | 0.34 | 70.00 | 0.36 |
| | Pore area fraction (%) | | | | | |
| PLM | 74.14$^a$ | (0.67) | 72.36$^a$ | (3.46) | 84.39$^b$ | (2.55) |
| CLSM | 74.74$^a$ | (1.22) | 75.39$^a$ | (3.74) | 83.57$^b$ | (0.13) |
| RM | 12.92$^c$ | (0.80) | 13.60$^c$ | (1.49) | 12.54$^c$ | (0.16) |
| | Fractal dimension (D) from image analysis | | | | | |
| PLM | 2.82$^a$ | (0.03) | 2.82$^a$ | (0.02) | 2.81$^a$ | (0.02) |
| CLSM | 2.89$^b$ | (0.003) | 2.81$^a$ | (0.01) | 2.83$^a$ | (0.02) |
| RM | 2.87$^b$ | (0.02) | 2.74$^c$ | (0.02) | 2.76$^c$ | (0.01) |
| | Fractal dimension (D) based on the weak-link regime | | | | | |
| | 2.63$^a$ | (0.01) | 2.59$^b$ | (0.01) | 2.60$^b$ | (0.01) |

Values in parentheses are standard deviation. For each type of analysis, means in the same row and column without a common letter are significantly different ($p < 0.05$).

**Table 2** Parameters of modified Avrami Model[a] of MG/HOSO oleogels as a function of the CTP used for their formation.

| | CTP corresponding to | | | | | |
|---|---|---|---|---|---|---|
| | 5 °C | | 17.5 °C | | 30 °C | |
| | Analysis from rheo-microscope images[b] | | | | | |
| $t_0$ (min) | 7.166 | (0.316) | 7.850 | (0.144) | 8.199 | (0.406) |
| $n$ | 1.839 | (0.164) | 1.784 | (0.205) | 1.934 | (0.108) |
| $k_{app}$ | 0.382 | (0.037) | 0.355 | (0.097) | 0.195 | (0.017) |
| $R^2$ | 0.99 | | 0.99 | | 0.96 | |
| | Analysis from rheology - cooling global process[c] | | | | | |
| $t_0$ (min) | 10.181 | (0.621) | 10.342 | (0.483) | 14.384 | (0.245) |
| $n$ | 1.371 | (0.005) | 1.494 | (0.066) | 0.962 | (0.040) |
| $k_{app}$ | 0.074 | (0.026) | 0.019 | (0.007) | 0.034 | (0.028) |
| $R^2$ | 0.994 | | 0.998 | | 0.983 | |
| | Analysis from rheology - crystals formation stage[d] | | | | | |
| $t_0$ (min) | 4.857 | (0.445) | 5.217 | (0.485) | 5.942 | (0.245) |
| $n$ | 2.230 | (0.396) | 2.121 | (0.192) | 2.008 | (0.145) |
| $k_{app}$ | 0.118 | (0.006) | 0.085 | (0.031) | 0.047 | (0.009) |
| $R^2$ | 0.983 | | 0.983 | | 0.989 | |

[a]Ys/Ymax = 1-exp (-$k_{app}$(t-$t_0$)$^n$). Ys/Ymax was computed as a function of: [b]the crystal area% determined from RM images; [c]the complex viscosity acquired during the entire cooling process; [d]the complex viscosity acquired during crystal formation stage (determined according to RM images).
Values in parentheses are standard deviation.

**Table 3** Elastic modulus (G') final value, oil binding capacity (OBC), and hardness (Ha) of MG/HOSO oleogels as a function of the CTP used for their formation.

| | CTP corresponding to | | | | | |
|---|---|---|---|---|---|---|
| | 5 °C | | 17.5 °C | | 30 °C | |
| G' (Pa) | $3.57 \times 10^{5a}$ | $(1.8 \times 10^4)$ | $8.46 \times 10^{5b}$ | $(4.9 \times 10^4)$ | $1.92 \times 10^{6c}$ | $(1.7 \times 10^4)$ |
| OBC (%) | $86.64^a$ | (0.76) | $83.27^b$ | (0.85) | $78.08^c$ | (0.93) |
| Ha (N) | $3.16^a$ | (0.12) | $2.88^b$ | (0.13) | $4.01^c$ | (0.16) |

Values in parentheses are standard deviation. Means in the same row without a common letter are significantly different ($p < 0.05$).

**Highlights**

- Monoglycerides oleogels were produced using different cooling temperatures profiles
- Rheomicroscopy was applied to evaluate crystal formation during gelation process
- The weak-link regime model for colloidal dispersion was applied to dynamic systems
- Images allow to obtain a more restricted time domain to analyze rheological data
- The obtained findings may serve to the food industry to tailoring oleogel's quality

Graphical abstract